ELSEVIER

Journal of Nuclear Materials 301 (2002) 153–164

journal of nuclear materials

www.elsevier.com/locate/jnucmat

Hydride blister formation in Zr–2.5wt%Nb pressure tube alloy ☆

R.N. Singh [a,*], R. Kishore [a], T.K. Sinha [a], B.P. Kashyap [b]

[a] *Materials Science Division, Bhabha Atomic Research Centre, Mumbai 400 085, India*

[b] *Department of Metallurgical Engineering and Materials Science, IIT Powai, Mumbai 400 076, India*

Received 2 August 2001; accepted 27 November 2001

Abstract

Hydride blisters were grown over a period of 5–91 days under controlled thermal boundary condition using Zr–2.5wt%Nb pressure tube sections. Rectangular plate type specimens were hydrided to hydrogen concentration in the range of 20–250 ppm by weight and homogenized at 400 °C. These specimens were held in a specially fabricated jig capable of producing the required thermal gradients. The bulk specimen and the cold spot temperatures were maintained in the range of 270–400 °C and 40–100 °C respectively. Depending on the thermal gradients employed, two types of blister morphology were identified. The type I blister was single, round and located at the cold spot region whereas the type II blister consisted of several small blisters along a ring around the cold spot. Microstructural examination of the blister cross-section revealed three regions; a single-phase region consisting of hydrides, a region consisting of matrix containing both radial and circumferential hydrides, and another region consisting of matrix and circumferential hydrides. An attempt was made to rationalize the observed radial–circumferential hydride platelet orientation. Hydride blister growth rates were found to vary strongly with hydrogen concentration and bulk specimen temperature. The observed time for blister growth was found to be in agreement with the Sawatzky's model [31]. © 2002 Published by Elsevier Science B.V.

1. Introduction

Dilute zirconium alloys are used as the core structural materials of pressurized heavy water reactors (PHWRs) [1–5] because of their adequate aqueous corrosion resistance, low neutron absorption cross-section, and good elevated temperature mechanical properties. Though the hydrogen content in the core components is kept as low as possible by controlling the manufacturing process parameters [6], they can pick up hydrogen (deuterium) during service [5,7]. Hydrogen present in excess of solid solubility precipitates out as brittle hydride phase and can severely limit the life of core components [3–5]. The hydrogen-related problems associated with these components are hydride embrittlement [5,8–12] due to stress reorientation of hydride [5, 13–20], delayed hydride cracking (DHC) [5,7,21–26] and embrittlement due to the formation of hydride blisters [27–35]. Though considerable work has been done on stress reorientation and DHC, and these are understood fairly well, all the aspects of blister formation are not yet clearly understood.

The formation of hydride blisters in zirconium alloy pressure tube (PT) should be visualized in conjunction with the arrangement of core components in PHWR. Fig. 1 shows a schematic of a section of PHWR. Horizontally oriented pressure tubes act as miniature pressure vessels in PHWR. A Calandria tube (CT) surrounds each pressure tube. Garter springs are provided at regular intervals in the annular space to support the pressure

☆ Part of this work has been published as BARC report no. BARC/2001/E/012.

* Corresponding author. Fax: +91-22 550 5239.

E-mail address: mms@apsara.barc.ernet.in (R.N. Singh).

0022-3115/02/$ - see front matter © 2002 Published by Elsevier Science B.V.
PII: S0022-3115(02)00708-0

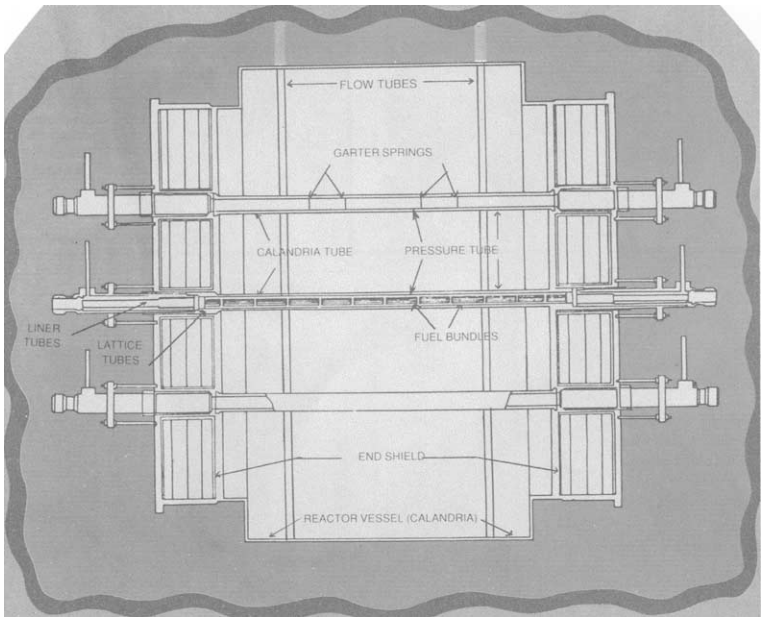

Fig. 1. Schematics of PHWR section showing the arrangement of the core components.

tube and prevent excessive sagging. Displacement of the garter springs from the designed location either during installation of the reactor or during service can lead to PT–CT contact and sets up a steep thermal gradient across the pressure tube. Hydrogen migrates down the temperature gradient [5,31]. Once the local solid solubility is exceeded the hydrogen precipitates out as hydride at or around the low temperature spot (henceforth called the cold spot). Since the transformation of zirconium metal into hydride is associated with an increase in volume, a bulge appears at the cold spot. This hydride bulge, due to its appearance, is called a hydride blister.

Attempts to contain the damage to the integrity of the pressure tubes due to hydride blister formation can be made from two angles [35]. Firstly, from the basic materials research point of view, the blister is modeled with various boundary conditions to evaluate the blister size, time to grow blisters of known size [31], growth rate [35], and hydrogen concentration profile [27]. The material properties like cracking strength of hydride blisters [32] can be used by designers. Secondly attempts are being made to demonstrate the capability of the non-destructive techniques (both intrusive and non-intrusive) in detecting the blisters formed in the contacting channels [35–38].

Recently the embrittlement due to hydride blister formation has received great attention due to its bearing on the safety and the life of the pressure tubes of the PHWRs [27–35]. A literature survey on hydride blister formation in dilute zirconium alloys [27–35] showed that the issues like the occurrence of different blister morphologies, the orientation of hydride platelets in the matrix surrounding the blister and the parameters affecting the kinetics of blister growth are yet to be resolved. In this work the possible mechanism of blister formation based on the metallographic features observed on the blister section, the role of stress [34] in governing the orientation of hydride platelets in the matrix surrounding the hydride blister, the blister formation threshold (BFT), the kinetics of blister growth and parameters affecting hydride blister growth rate and blister morphologies are being reported.

2. Experimental procedure

Zr–2.5wt%Nb alloy was obtained in the form of pressure tube spools of length 130 mm, internal diameter 103 mm and wall thickness 4.7 mm in the autoclaved condition. The composition analysis indicated Nb and oxygen contents to be 2.54% and 1000 ppm by wt respectively. The plate type specimens of length 35–100 mm, width 15–25 mm and thickness 0.5–4.5 mm, were obtained from cold flattened tube sections. These specimens were polished successively up to 1200 grit emery paper and subsequently were gaseously charged with a controlled amount of hydrogen in a modified Sivert's apparatus at a temperature in the range 370 °C. A homogenization treatment was given at the 400 °C for 24 h to attain uniform distribution of hydrogen.

Hydride blisters were grown following two methodologies. In case I the specimens were soaked at a pre-

Table 1
Details of hydride blisters grown in zirconium alloy for selected specimens

Specimen id.	Material	Hydrogen content in wt ppm	Soaking time in hours	Thermal boundary condition (°C) (T_b/T_{cs})	Duration in days	Morphology type
B0	Zr–2.5wt%Nb PT alloy	20	1	300/40	91	Type I
B1	Zr–2.5wt%Nb PT alloy	250	0	270–290/50–70	17	Type II
B2	Zr–2.5wt%Nb PT alloy	195	0	300–330/50–70	30	Type II
B3	Zr–2.5wt%Nb PT alloy	230	1	330–350/50–70	18	Type I
B4	Zr–2.5wt%Nb PT alloy	110	1	380–390/50–70	31	Type I
B5	Zr–2.5wt%Nb PT alloy	240	0	330–340/50–70	20	Type II
B6.1	Zr–2.5wt%Nb PT alloy	218	1	300/50–55	5	Type I
B6.2	Zr–2.5wt%Nb PT alloy	218	0	300/45–50	7	Type II
B7	Zircaloy-2 PT	118	0	300/60–80	28	Type II
B8	Zr–2.5wt%Nb PT alloy	135	1	$270 \pm 10/100 \pm 10$	20	Type I
B9	Zr–2.5wt%Nb PT alloy	75	1	$275 \pm 5/55 \pm 15$	120	Type I

determined temperature for 1 h so as to take all the hydrogen into solution and a cold spot was formed using a water-cooled copper cone. This ensured that no hydride precipitate was present near the contact region before it was made a cold spot. In case II the cold finger was maintained in contact with the specimens from the beginning of heating. This ensured that the hydride platelets were present in the region around the cold spot before the arrival of the thermally migrated hydrogen. The specimen identity, hydrogen content and thermal boundary conditions of blister growth for selected specimens are listed in Table 1. For temperature measurement and to record the temperature profile as a function of distance from the cold spot, K-type thermocouples were placed on both faces of the samples at regular interval. The details of both the hydrogen charging system and the blister simulation jig are described in Appendices A and B respectively.

Optical microscopy was used to reveal the microstructure of some of the hydrided specimens and a few hydride blister sections along the radial–circumferential plane of the pressure tubes. The blister bulge height was measured using a micrometer with a resolution of 0.01 mm (i.e. 10 μm). Hydride blister growth rate was taken as the ratio of the bulge height of the blisters above the specimen surface to the time taken for growing it. The hydride blisters were also examined by neutron radiography.

3. Results

Fig. 2 shows the optical micrographs of the as-hydrided Zr–2.5wt%Nb pressure tube material containing (a) 35 ppm, (b) 60 ppm and (c) 85 ppm by weight of hydrogen along the radial–circumferential plane of the tube. The traces of hydrides can be seen as dark lines in this figure. This is expected as the microstructure and the texture of the pressure tube is such that only circumferential hydrides (oriented along the axial–circumferential plane of the pressure tube) form in the as-hydrided condition [5]. It may be noted that with an increase in hydrogen concentration the hydride platelet length is found to increase, though there is no significant change in interplatelet spacing.

Examination of the blisters suggested two distinct types of morphology (Fig. 3). In case I soaking temperature and time were so chosen that all the hydrogen was present in solution. The cold spot was established on the specimen after 1 h of soaking. This resulted in the formation of a single blister at the cold spot, designated as a type I blister (Fig. 3(a)). In case II, the cold finger was kept in contact with the specimen from the commencement of heating. This ensured that the region around the cold spot remained at lower temperature during heating. This led to the formation of several small blisters on a ring around the cold spot, which were termed type II blisters (Fig. 3(b)). With increasing time, these small blisters joined to form a continuous ring. The specimen identity, hydrogen contents and thermal boundary conditions for blister growth of these specimens are listed in Table 1.

Hydride blisters of type I could be detected easily by neutron radiography. Fig. 4 shows some of the typical neutron radiographs. Dark circular spots (marked by arrows) are the images of the various hydride blisters. However, the type II blister grown for the same duration could not be detected by neutron radiography.

The parameters like cold spot temperature, soaking temperature, specimen dimensions, contact conductivity, hydrogen content and alloy composition affect the hydride blister growth rate. Fig. 5(a) shows the effect of soaking temperature on blister growth rate for a given hydrogen concentration and cold spot temperature. With increase in soaking temperature, blister growth rate was observed to increase. The effect of hydrogen

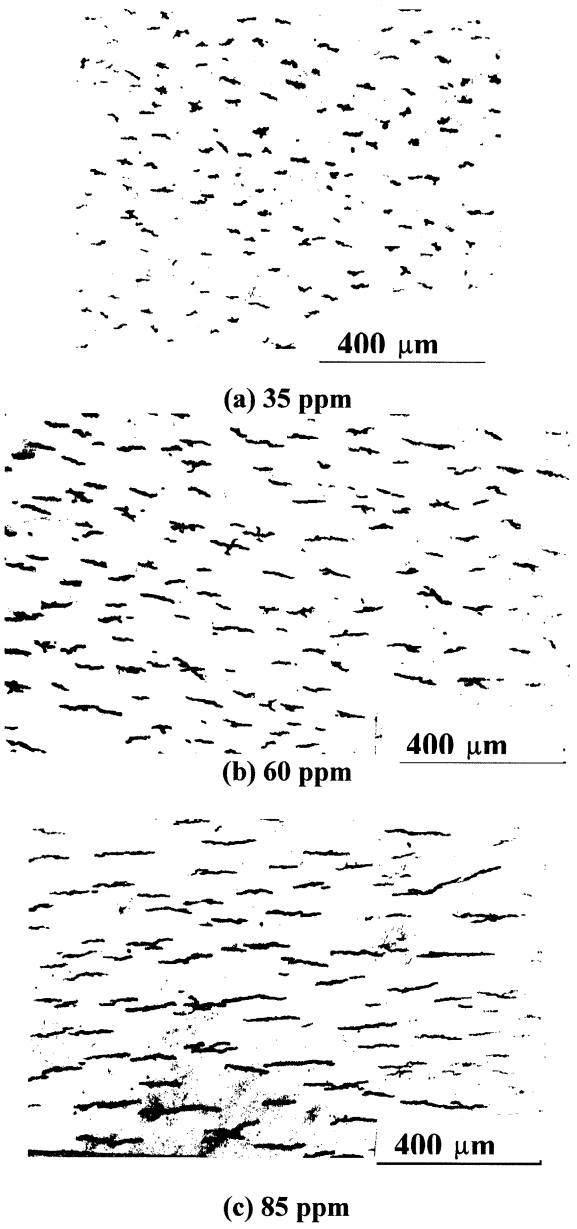

Fig. 2. Optical micrographs of as-hydrided Zr–2.5wt%Nb pressure tube material containing (a) 35 ppm, (b) 60 ppm and (c) 85 ppm (by weight) of hydrogen along the radial–circumferential plane of the tube. With increase in hydrogen concentration hydride platelet length is found to increase, though there is no significant change in interplatelet spacing.

content on the blister growth rate, for a given combination of bulk specimen and cold spot temperatures, has been shown in Fig. 5(b). In the hydrogen concentration range studied, the blister growth rate increases with the increase in hydrogen concentration.

Fig. 6(a)–(c) shows the radial–circumferential (RC) sections of hydride blisters grown in Zr–2.5wt%Nb pressure tube material. The metallographic examination of the section of types I (Fig. 6(a)) and II (Fig. 6(b) and (c)) blisters revealed a difference in their aspect ratio. Hydride platelets radiating from cold spot center can be seen. It is evident from this figure that a section of hydride blister can be classified into three regions (marked in Fig. 6(c)). Far from the center of blister is region I, comprising of matrix and circumferential hydrides. This region is similar to the micrograph (RC plane) obtained for the as-hydrided specimens (Fig. 2). As one approaches the center of blister, a region comprising of matrix, circumferential and radial hydrides can be seen. This is marked as region II (Fig. 6(c)). Region III is the region of single-phase hydride. The boundary between regions II and III appears darker under the optical microscope because of uneven etching [27,28]. Single-phase region III etches evenly and appears brighter. In region II (Fig. 6(c)), both radial and circumferential hydrides can be seen forming finer network as one approaches the boundary between regions II and III.

4. Discussion

Hydride blister formation were studied in Zr–2.5wt%Nb pressure tubes of the Indian PHWRs, which are manufactured [39] by a route similar to the modified route II of Atomic Energy of Canada Limited [40]. The modified route II [40] consists of two cold working steps (instead of one cold working step for conventional route) and an intermediate annealing step. Lower extrusion ratio employed in modified route compared to the conventional route ensures lower aspect ratio of α grains, less intense circumferential basal pole texture and more uniform microstructure resulting in improved irradiation resistance, reduced susceptibility to stress reorientation of hydrides and uniform mechanical properties across the length of the tube [39]. In this section some of the results obtained from the out-of-pile hydride blister simulation experiments carried out under controlled thermal boundary conditions are compared with those reported in earlier investigations [27–35]. Hydride blister morphology, the influence of hydrogen content and soaking temperature on blister growth rate, reorientation of the hydride platelet [5,17] in the matrix surrounding the blister, threshold hydrogen concentration for blister formation (BFT), effect of soaking and cold spot temperature on BFT, and Sawatzky's model [31] of blister growth are discussed in the following.

4.1. Hydride blister morphologies

The two types of blister morphology, types I and II, obtained in the present investigation (Fig. 3) are similar

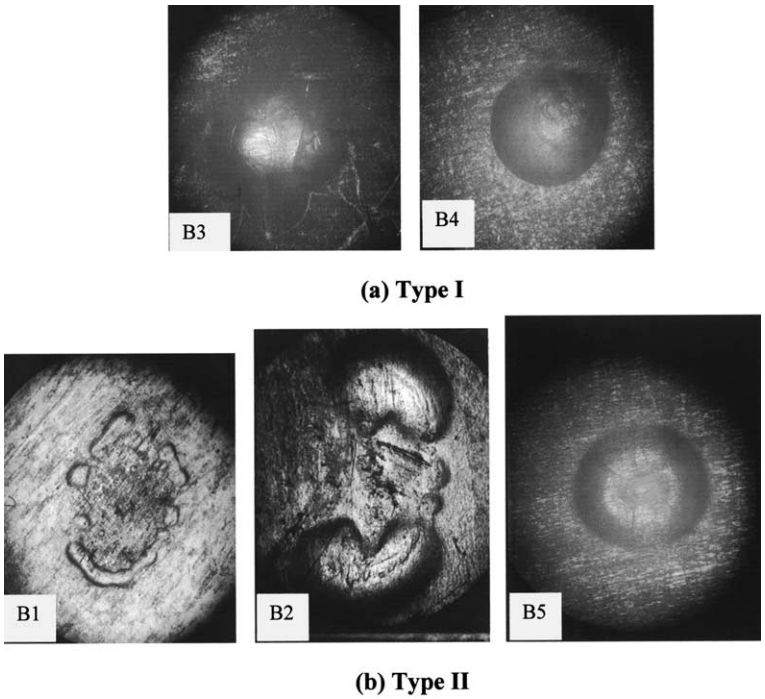

Fig. 3. Top view of the hydride blisters grown in Zr–2.5wt%Nb pressure tube alloy. Both (a) type I and (b) type II blisters can be seen. In one case single blisters formed at the cold spot and was termed as type I whereas in another case several small blisterets formed on a ring around cold spot and were termed as type II. With time, the small blisterets of type II morphology joined together to form a ring. (See Table 1 for designations.)

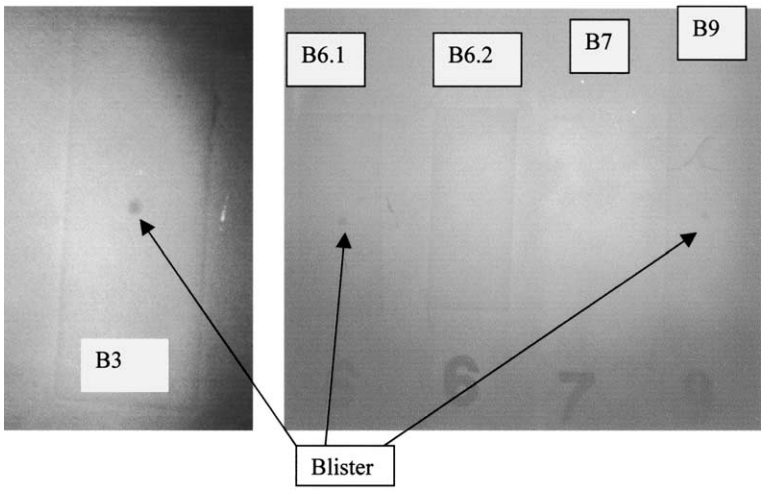

Fig. 4. The neutron radiographs of types I and II blister, grown in zirconium alloy pressure tube material. Details of the samples are given in Table 1.

to those reported by Domizzi et al. [27]. Formation of type II blister was attributed [27] to improper contact, which may be due to the large size of the cold finger (7 mm). However, results of the present investigation indicated that the formation of single or multiple blisters, using a cold finger size of 2 mm only, is a function of soaking time, thermal boundary condition and hydrogen content. The specimens which were soaked for an hour, led to the formation of single blisters, whereas the one without any soaking resulted in the formation of multiple

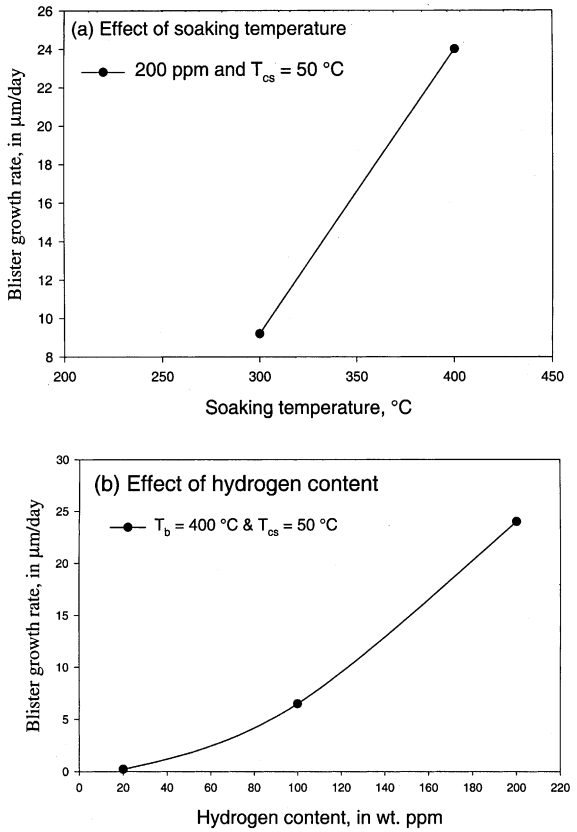

Fig. 5. Variation of blister growth rate with (a) soaking temperature and (b) hydrogen content (in weight ppm).

blisters around the cold spot. Multiple blisters could be more readily grown on thinner plates, at very low cold spot temperature and for high hydrogen content. Since in all the cases the contact of the cold finger and specimens were very good, type II blister are unlikely to have formed due to improper contact. A possible reason for type II blister formation is proposed below.

In case I, after soaking, all the hydrogen was in solution, and when the cold finger was brought into contact, the region of specimen in contact with the cold finger cooled first. With the decrease in the temperature in this region, the hydrogen in excess of solid solubility precipitated as hydride. This hydride acted as the nucleus and kept growing with the diffusion of thermally migrated hydrogen from the bulk. However, in case II, due to insufficient soaking and/or high hydrogen content all the hydrides were not dissolved. The undissolved hydride platelets in the region around the cold spot acted as the nuclei. Thus with the arrival of thermally migrated hydrogen, the undissolved hydride platelets could have grown simultaneously. With time these individual blisterets grew till they meet each other and gave the appearance of a ring around the cold spot. This was the reason for the formation of a single blister at the cold spot in case I (Fig. 3(a)) and several small blisters on a ring around the cold spot in case II (Fig. 3(b)).

Since hydride blisters are formed in zirconium alloys due to the thermal migration of hydrogen down the thermal gradient to the cold spot [31], any metallurgical/mechanical parameter, which affects the diffusion (or temperature gradient) will have a significant influence on blister morphology and its growth rate. Some of these parameters are bulk specimen temperature, soaking time, cold spot temperature, geometry of cold finger, thickness of plate, volume fraction of alpha and beta phases, mechanical and crystallographic anisotropy and alloying elements. The effect of a few such variables are elaborated below.

Blisters were grown with bulk specimen temperature in the range of 270–400 °C. Though the bulk specimen temperature seemed to have no effect on the morphology of the blisters, it was found to affect the kinetics of the process. At higher temperature it took shorter time to grow a blister of given size (Fig. 5(a)). This is expected, because at higher temperatures not only the amount of hydrogen diffusing is higher due to the endothermic nature of terminal solid solubility of hydrogen in zirconium alloys [41] but also due to faster hydrogen migration. Hence, for higher soaking temperatures and for higher hydrogen content the blister growth rate is expected to be higher, which can be inferred from Fig. 5(a) and (b). Soaking the specimens favors the formation of type I blisters whereas type II blisters formed when the soaking was not employed (Table 1). The kinetics of type II blister formation are slower; blisters grown for same duration were smaller compared to type I. This small size was probably the reason for their non-detectibility in neutron radiographs (Fig. 4).

4.2. Hydride platelet orientation around blister

As can be seen in Fig. 6(c), radial hydrides appear only in a location around the deepest point (marked by ◯) of the blister. Near the surface on both sides of the blister (Fig. 6(c)) no radial hydrides could be seen. The microstructure and the texture of the matrix region surrounding the blister are expected to remain unchanged. Hence these factors [5,42] could not explain the variation in hydride platelet orientation in the matrix around the blister. Since the hydride platelet orientation in Zr–2.5 wt%Nb alloy is governed by stress [13–20], the stress field generated as a result of blister formation [27,34] may explain the occurrence of radial hydrides only at selected locations.

In this section a qualitative model is presented to explain the formation of the hydride platelet network in the matrix surrounding the blister. In the initial stage of blister formation, only circumferential hydrides are formed governed by the crystallographic criteria [5,42].

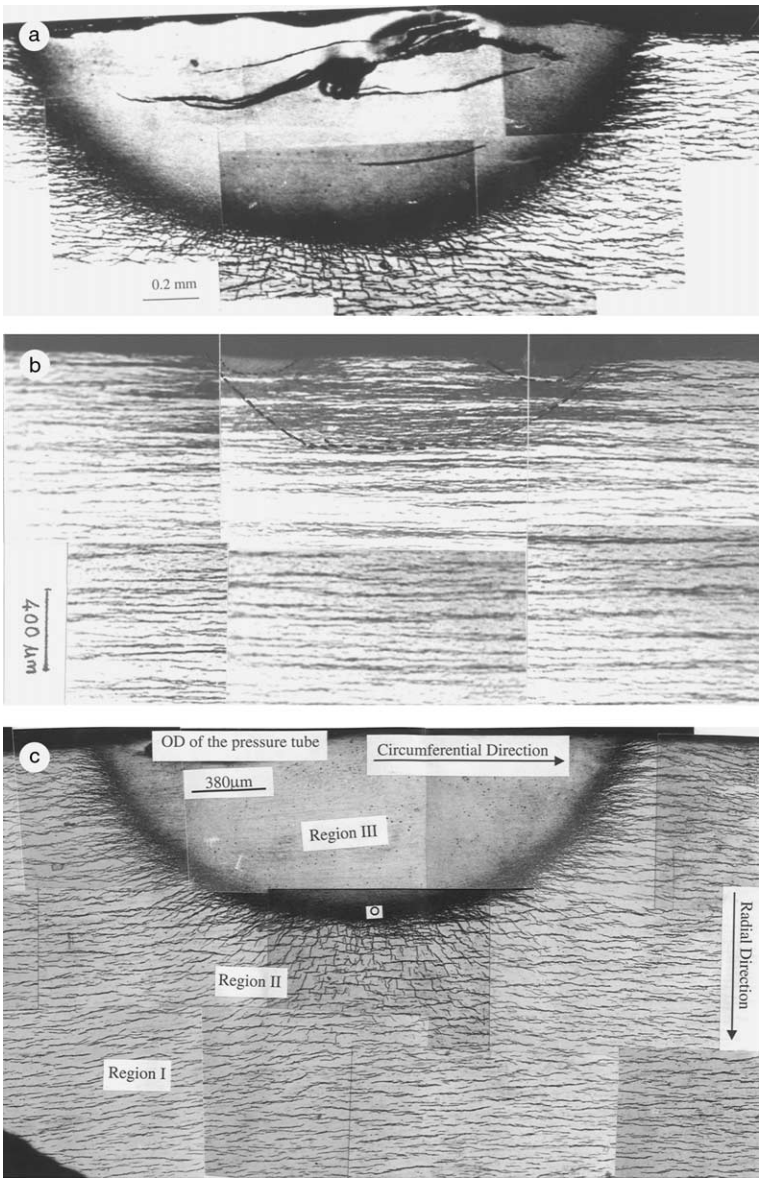

Fig. 6. Optical micrograph of the radial–circumferential (RC) section of hydride blister, grown in Zr–2.5wt%Nb pressure tube material under laboratory condition. The blister sample shown in Fig. 3 was sectioned along radial circumferential plane. (a) Type I—specimen Id. B3, (b) type II—specimen Id. B2 shows the hydride distribution in the initial stages of blister growth and (c) type II—specimen id. B5 shows hydride platelet orientation at an advanced stage of blister growth. Three regions have been marked in (c). Region I consists of matrix containing circumferential hydrides, region II of matrix containing both radial and circumferential hydrides and region III consists mainly of δ-hydride.

During this stage of blister growth, with the arrival of thermally migrated hydrogen to the cold spot region, the interplatelet spacing decreases and the matrix gradually transforms into single-phase hydride called a blister. As the blister grows, the matrix surrounding the blister experiences two types of stresses. These are local and global stresses. The local stress, σ_{lo}, originates because of the accommodation [43] of the individual hydride platelets in the matrix. The component of σ_{lo} normal to the hydride platelet is compressive in nature for the matrix as it is sandwiched between two hydride platelets [29]. As the interplatelet spacing decreases (and/or the platelet thickness increases), the magnitude of this compressive stress is expected to increase. The global stress component, σ_{gl}, [34] is generated due to the volume mismatch between the single-phase hydride (region

III of blister) and the matrix surrounding it (Fig. 6(c)). Since hydrides occupy more volume than the metal from which it forms, the matrix region surrounding the blister experiences dilatation along the in-plate direction resulting in setting up of the stress field in the matrix. This stress is expected to have a higher magnitude and long range influence [34] compared to the local stress described earlier. The hydride platelet orientation at any location in the matrix around the blister is governed by sum of both the global and local stresses. Once the total tensile stress prevailing at any point in the matrix is greater than the threshold stress for reorientation of hydrides [5,13–20], radial hydride precipitates out. The magnitude of the stress prevailing at the hydride platelet–matrix interface is reported to be around 85–115 MPa [44], which is much lower than the threshold stress for reorientation of hydrides (~200 MPa at 300 °C) in this alloy [17]. As one moves away from the interface this stress is expected to decrease as inverse of distance. Thus the local stress alone cannot explain the formation of radial hydrides and it is felt that the global stress played a dominant role in the formation of radial hydrides in the matrix surrounding the blister.

4.3. Blister formation threshold

Hydrogen is known to migrate down the concentration and the temperature gradient and up the tensile stress gradient [5]. The general diffusion equation [5] using all the three parameters for a cylindrically symmetric temperature distribution is given below:

$$J = \frac{-DC_r}{RT}\left[RT\frac{\mathrm{d}\ln C_r}{\mathrm{d}r} + \frac{Q^*}{T}\frac{\mathrm{d}T}{\mathrm{d}r} - \frac{V^*}{3}\frac{\mathrm{d}\sigma}{\mathrm{d}r}\right], \tag{1}$$

where J is hydrogen flux, D is diffusion coefficient of hydrogen in α-zirconium [31]

$$= D_0 \exp\left(\frac{-Q}{RT}\right) = 7.52\times 10^{-2}\exp\left(\frac{-7564}{RT}\right),$$

C_r is hydrogen concentration at any point r participating in diffusion = terminal solid solubility (TSS), for bulk hydrogen concentration > TSS [31]

$$= A\exp\left(\frac{-H_m}{RT}\right) = 1.99\times 10^5\exp\left(\frac{-9300}{RT}\right).$$

For type I blister [45]

$$\mathrm{TSS} = \mathrm{TSSP} = 4.11\times 10^4\exp\left(\frac{-6698.6}{RT}\right)$$

and for type II blister [45]

$$\mathrm{TSS} = \mathrm{TSSD} = 6.86\times 10^4\exp\left(\frac{-8020}{RT}\right).$$

TSSP is terminal solid solubility for precipitation [45,46], TSSD is terminal solid solubility for dissolution [45,46], R is gas constant, T is absolute temperature, Q^* is heat of transport of hydrogen in metal, V^* is volume of transport of hydrogen in metals, σ is stress tensile (taken as +ve) and compressive (taken as −ve).

As can be seen from the general diffusion equation given above, hydrogen migrates down the temperature gradient. Let us take the case when bulk hydrogen concentration is more than the TSS at the cold spot temperature. In such a case, imposition of a thermal gradient will also lead to the setting up of a concentration gradient, and both the thermal and the concentration gradients ensure that hydrogen migration takes place towards the cold spot [31]. However, for the case when bulk hydrogen concentration is lower than the TSS at the cold spot temperature, initially hydrogen migration due to thermal gradient takes place. This sets up a concentration gradient, which will allow hydrogen migration away from the cold spot. This has been illustrated in Fig. 7(a)–(c). Hence, there must exist a critical hydrogen concentration for a given thermal boundary condition, below which no net migration of hydrogen takes place. At this concentration of hydrogen a dynamic equilibrium is attained and the hydrogen flux due to concentration gradient and thermal gradient acts against each other. This thermal migration threshold is referred to as the BFT [28].

In the absence of stress and under the above mentioned dynamic equilibrium, the net flux J is given by

$$J = \frac{-DC_r}{RT}\left[RT\frac{\mathrm{d}\ln C_r}{\mathrm{d}r} + \frac{Q^*}{T}\frac{\mathrm{d}T}{\mathrm{d}r}\right] = 0. \tag{2}$$

Solving this partial differential equation, one can find the threshold hydrogen concentration as shown below.

From Eq. (2), we get

$$\begin{aligned}
&RT\frac{\mathrm{d}\ln C_r}{\mathrm{d}r} + \frac{Q^*}{T}\frac{\mathrm{d}T}{\mathrm{d}r} = 0\\
&\Rightarrow \frac{1}{C_r}\frac{\mathrm{d}C_r}{\mathrm{d}r} + \frac{Q^*}{RT^2}\frac{\mathrm{d}T}{\mathrm{d}r} = 0\\
&\Rightarrow \frac{1}{C_r}\frac{\mathrm{d}C_r}{\mathrm{d}T}\frac{\mathrm{d}T}{\mathrm{d}r} + \frac{Q^*}{RT^2}\frac{\mathrm{d}T}{\mathrm{d}r} = 0\\
&\Rightarrow \frac{1}{C_r}\frac{\mathrm{d}C_r}{\mathrm{d}T} + \frac{Q^*}{RT^2} = 0.
\end{aligned}$$

Separating the variables and on integrating between bulk hydrogen concentration (C_b) and TSS at cold spot temperature (TSS_cs) we get

$$\int_{C_\mathrm{b}}^{\mathrm{TSS}_\mathrm{cs}}\frac{\mathrm{d}C_r}{C_r} = -\frac{Q^*}{R}\int_{T_\mathrm{b}}^{T_\mathrm{cs}}\frac{\mathrm{d}T}{T^2}$$

where T_b is the bulk specimen temperature.

Therefore

$$\frac{\mathrm{BFT}}{\mathrm{TSS}_\mathrm{cs}} = \exp\left(-\frac{Q^*}{R}\frac{(T_\mathrm{b}-T_\mathrm{cs})}{T_\mathrm{b}T_\mathrm{cs}}\right) \tag{3}$$

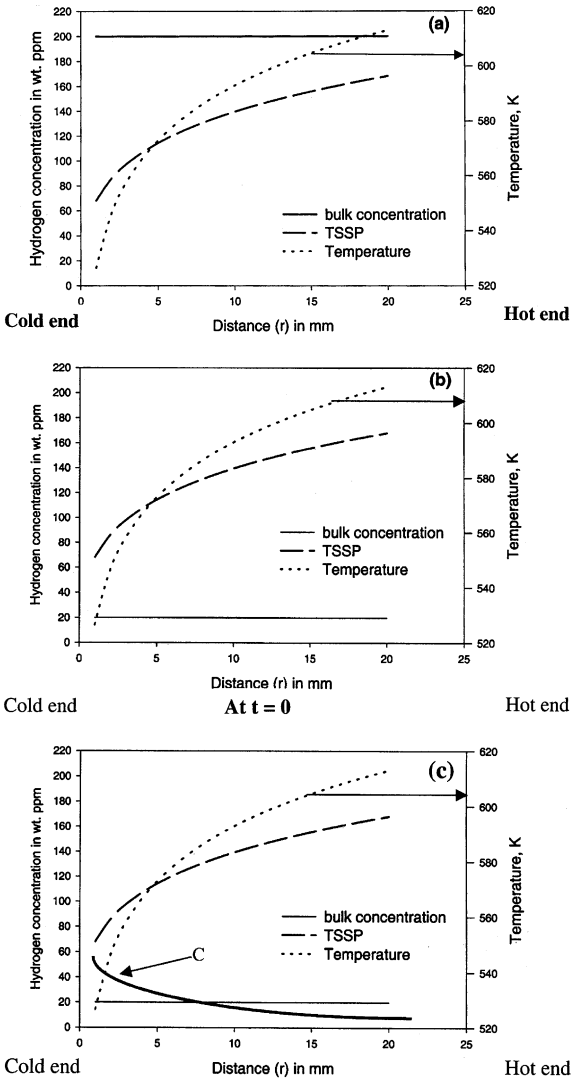

Fig. 7. The variation of temperature and concentration across the cold spot and hot end of the specimen. For $C_b > TSS$ at cold spot, imposition of thermal gradient results in setting up of concentration (TSS) gradient as well (a) and for $C_b < TSS$ at cold spot, imposition of thermal gradient does not result in setting up of concentration gradient at $t = 0$ (b). However, with time as thermal migration of hydrogen starts, concentration gradient builds up which opposes the hydrogen migration due to thermal gradient (c).

Thus, BFT can be evaluated using Eq. (3). From this equation it is evident that BFT depends on terminal solid solubility at cold spot temperature, heat of transport of hydrogen in α-Zr phase, cold spot and bulk specimen temperatures. As TSS depends on direction of approach of temperature [45], BFT will also depend on the direction of approach of temperature. Fig. 8(a) and (b) shows the BFT/TSS_{cs} and BFT variation with cold spot and

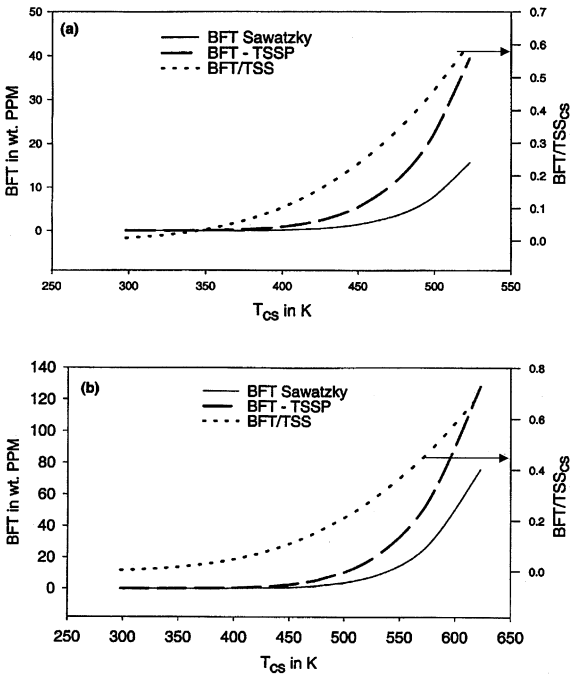

Fig. 8. Variation of BFT with cold spot temperature for soaking temperature of (a) 300 °C (573 K) and (b) 400 °C (673 K).

bulk specimen temperatures plotted using Eq. (3). The computation was carried out for cold spot temperature ranges of 293–523 (Fig. 8(a)) and 293–623 K (Fig. 8(b)) using bulk specimen temperatures of 573 and 673 K respectively. For a given bulk specimen temperature, as the cold spot temperature increases BFT is predicted to increase. The BFT value computed using TSSP [45] is higher than that computed using TSSD [45]. The BFT decreases with increase in bulk specimen temperature for a given cold spot temperature (Fig. 8(a) and (b)).

4.4. Sawatzky's model [31]

The model developed by Sawatzky was applied to the blisters grown under laboratory conditions in the present study. By considering logarithmic temperature distribution, the above model was used to estimate the time required for blister growth.

4.4.1. Estimation of hydrogen flux

Assuming cylindrically symmetric temperature distribution, as in the present case, the thermomigration equation describing the hydrogen flux at any point is given by

$$J = -D\frac{dC_r}{dr} - \frac{DC_rQ^*}{RT^2}\frac{dT}{dr}, \quad (4)$$

where the symbols have the same meaning as in Eq. (1).

Therefore,

$$\frac{dC_r}{dr} = \frac{d(TSS)}{dr} = \frac{AH_m}{RT^2} \exp\left(\frac{-H_m}{RT}\right) \frac{dT}{dr}. \quad (5)$$

The mid-wall temperature distribution can be approximated as

$$T = T_0 + K_p \ln(r) \quad \text{or} \quad \frac{dT}{dr} = \frac{K_p}{r}. \quad (6)$$

Using Eqs. (5) and (6), Eq. (4) can rewritten as

$$J = -\frac{D_0 A K_p}{rT^2} \left(\frac{H_m + Q^*}{R}\right) \exp\left(-\frac{H_m + Q}{RT}\right). \quad (7)$$

4.4.2. Estimation of time for blister formation

Amount of hydrogen in blister, M, is given by $M = VC_\delta$, where V is the volume of blister and C_δ is hydrogen concentration in δ-hydride.

$$M = \frac{2}{3}\pi r_0 b C_\delta, \quad (8)$$

where blister dimensions r_0 and b are defined in Fig. 9.

If $J(r_0)$ be the flux at $r = r_0$,

$$M = 2\pi r_0 w J(r_0) t. \quad (9)$$

From Eqs. (8) and (9) we get

$$t = \frac{r_0 b C_\delta}{3wJ(r_0)}. \quad (10)$$

The time for growing a blister of given size was calculated using the values of constants given in Table 2. As can be seen from Table 2, the estimated time, as per Eq. (10) and using the TSS value cited by Sawatzky [31], is higher than the experimental value. However, it should be noted that for type I blisters cold spot temperature was approached from higher side and for type II blisters cold spot temperature was approached from lower side. Thus, for computation of time using Eq. (10), when TSSP [45,46] was used for type I blisters and TSSD [45,46] was used for type II blisters, the estimated time was closer (within 50%) to the experimental value. Considering the following reasons, the agreement between the actual time for blister growth and that predicted by the analytical model [31] (Table 2) can be considered good.

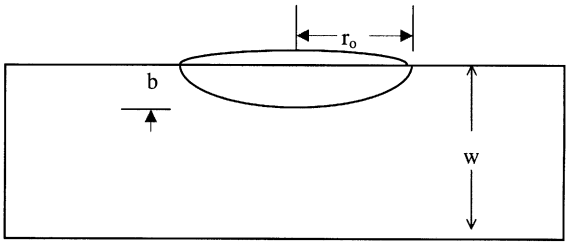

Fig. 9. Definition of blister dimensions used in Sawatzky's model [31].

1. The uncertainty in the diffusion co-efficient of the hydrogen in this alloy [31,45,46].
2. The assumption that average flux is a function of mid-wall temperature [31]. The contribution from the high temperature half of the specimen thickness should be greater than that from the low temperature half.
3. The contribution from the hydrogen migration up the stress gradient due to the blister growth was not considered.

All these factors will affect the hydrogen flux, which influences the estimated time for blister growth as predicted by the above model.

5. Conclusions

1. Two types of hydride blister morphology were identified. The presence or absence of hydrides before the arrival of thermally migrated hydrogen was found to be responsible for the development of these morphologies. Neutron radiography could detect type I blisters only as type II blisters were small.

Table 2
Comparison of estimated time to grow a blister of given size with actual experimental value

S. no.	Details	B3	B5
1	Type of blister morphology	I	II
2	r_0 in mm	1.57	1.56
3	b in mm	1.17	1.31
4	W in mm	2.7	4.44
5	Cylindrically symmetric mid-wall temperature profile for $1.0 < r < 20$ mm	$T = 526.5 + 28.9 \ln r$	$T = 529.1 + 26.3 \ln r$
6	t in days based on TSS $= 1.99 \times 10^5 \exp\left(\frac{-9300}{RT}\right)$ [31]	38	27.2
7	t in days based on TTSP for type I and TSSD for type II [45]	19.6	26.1
8	Actual	18	20
9	For $Q^* = 6000$ cal/mol and $C_\delta = 101$ μg/mm^3 [31]		

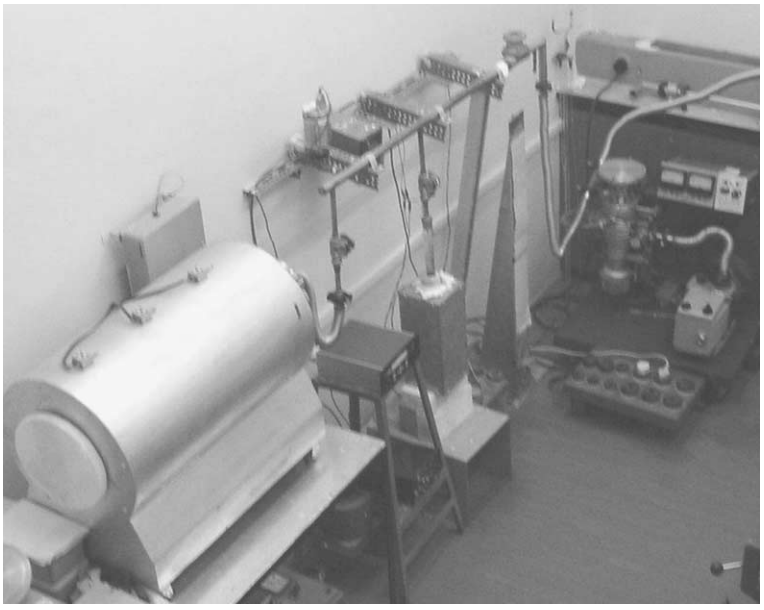

Fig. 10. Photograph of gaseous hydrogen charging facility.

2. For a given cold spot temperature and hydrogen concentration, blister growth rate increases with increase in soaking temperature.
3. The hydride platelet orientation in the matrix surrounding the blister was rationalized in terms of the stresses generated in the matrix as a result of blister growth. However, its quantification in terms of blister shape and size, hydride interplatelet spacing and platelet aspect ratio needs further work.
4. For a given bulk specimen temperature, as the cold spot temperature increases, BFT is predicted to increase. The BFT decreases with increase in bulk specimen temperature for a given cold spot temperature.
5. The estimated time for blister growth according to Sawatzky's model is in good agreement with the experimental value.

Acknowledgements

Authors appreciate the constant encouragement provided by Dr S. Banerjee, Director, Materials Group. The technical assistance extended by N.T. Parekh and P.G. Adiga of Materials Science Division is acknowledged.

Appendix A. Hydrogen charging system

This system consists of two glass chambers to hold the specimen and the hydrogen source, a vacuum pumping system, a capacitance-based manometer and a couple of resistance heated furnace to heat the specimen and the hydrogen source. The photograph of the gaseous hydrogen charging facility is shown in Fig. 10. Pressure tube spools of length up to 200 mm can be

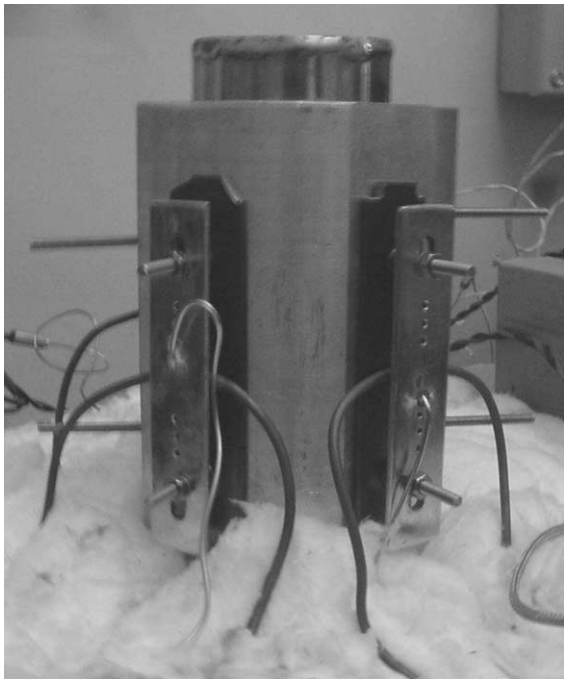

Fig. 11. Photograph of the multiple-specimen jig is shown in this figure. Water-cooled point contact used to form the cold spot can also be seen.

charged with controlled amount of hydrogen in a manner, which ensures that the initial microstructure remains unchanged. Pure zirconium hydride is used as source for hydrogen. Unlike electrolytic charging and LiOH autoclaving, this is a contamination free process and ensures uniformity of hydrogen distribution.

Appendix B. Blister simulation jig

It consists of a rod type resistance heater, aluminum jig, cold fingers of different sizes, temperature controllers and indicators and an insulation box. All these components are mounted on working table, called blister simulation bench. The aluminum jig is used for mounting the specimen(s) on which blisters are to be grown and the thermocouples at the predetermined locations for temperature profile measurement. Fig. 11 shows the photograph of the multiple-specimen jig mounted on the blister simulation bench. Three numbers of both curved and plate type test specimens can be loaded simultaneously on the multi-specimen jig for blister growth.

References

[1] E.F. Ibrahim, B.A. Cheadle, Can. Metall. Q. 24 (3) (1985) 273.
[2] C.D. Williams, Reactor Technol. 13 (2) (1970) 147.
[3] C.E. Ells, The Met. Soc. CIM, Annual Volume (1978) 32.
[4] D.P. Dautovich, M.G. Hay, P. Meyer, B. Mukherjee, H.J. Westwood, The Met. Soc. CIM, Annual Volume (1978) 45.
[5] D.O. Northwood, U. Kosasih, Int. Met. Rev. 28 (2) (1983) 92.
[6] J.R. Theaker, R. Choubey, G.D. Maon, S.A. Aldridge, L. Davis, R.A. Graham, C.E. Coleman, in: E.R. Bradley, G.P. Sabol (Eds.), Zirc in Nucl. Industry: 10th International Symposium, ASTM-STP-1245, 1994, p. 221.
[7] R.N. Singh, R. Kishore, S. Roychaudhury, M. Unnikrishnan, T.K. Sinha, P.K. De, S. Banerjee, Santosh Kumar, BARC report: BARC/2000/E/-038.
[8] K.S. Chan, Acta Metall. Mater. 43 (12) (1995) 4325.
[9] J.B. Bai, C. Prioul, S. Lansiart, D. Francois, Scripta Metall. Mater. 25 (1991) 2559.
[10] D. Wappling, A.R. Massih, P. Stahle, J. Nucl. Mater. 249 (1997) 231.
[11] J.B. Bai, C. Prioul, D. Francois, Metall. Mater. Trans. A 25 (1994) 1185.
[12] K.S. Chan, J. Nucl. Mater. 227 (1996) 220.
[13] P.K. Dey, J.T. John, V.V. Raman, S. Banerjee, J. Nucl. Mater. 203 (1993) 94.
[14] R.L. Eadie, C.E. Coleman, Scripta Metall. 23 (1989) 1865.
[15] G.W. Parry, AECL report no. 2624, 1966.
[16] M. Leger, A. Donner, Can. Metall. Q. 24 (3) (1985) 235.
[17] L.G. Bell, R.G. Duncan, AECL report no. 5110, 1975.
[18] J.B. Bai, C. Prioul, D. Francois, J. Adv. Sc. 3 (4) (1991) 188.
[19] D. Hardie, M.W. Sanahan, J. Nucl. Mater. 55 (1975) 1.
[20] C. Ells, J. Nucl. Mater. 35 (1970) 306.
[21] B. Cox, J. Nucl. Mat. 170 (1990) 1.
[22] K.F. Amouzouvi, L.J. Clegg, Metall. Trans. A 18 (1987) 1687.
[23] C.E. Coleman, AECL report no. 5260, 1976.
[24] R.L. Eadie, R.R. Smith, Can. Metall. Q. 27 (3) (1988) 213.
[25] L.A. Simpson, K. Nuttall, in: A.L. Lowe Jr., G.W. Parry (Eds.), Zirc. in Nucl. Industry, ASTM STP-633, 1977, p. 608.
[26] R.N. Singh, R. Kishore, T.K. Sinha, S. Roychaudhury, P.K. De, S. Banerjee. Prog. report no. BARC.MS-D.IAEA.2000.01 submitted at 2nd RCM, Pitesti, Romania, 5–9 June 2000.
[27] G. Domizzi, R.A. Enrique, J. Ovejero-Gracia, G.C. Buscaglia, J. Nucl. Mater. 229 (1996) 36.
[28] E.G. Price, IAEA Tech. Committee Meeting, February 1994, Mumbai, India.
[29] G. Domizzi, G. Vigna, S. Bermudez, J. Ovejero-Gracia, J. Nucl. Mater. 275 (1999) 255.
[30] M. Leger, T.P. Byrne, A.C. Wallace, D.V. Leemans, Ont. Hydro Res. Rev. No. 8 (1993) 46.
[31] A. Sawatzky, Can. Metall. Q. 24 (3) (1985) 227.
[32] M.P. Puls, Metall. Trans. A 19 (1988) 2247.
[33] H.D. Mair, M.D.C. Moles, M.P. Dolbey, IAEA Tech. Committee Meeting, February 1994, Mumbai, India.
[34] M.L. Vanderglas, Y.J. Kim, Int. J. Press. Vessels Piping 22 (1986) 177.
[35] R.N. Singh, R. Kishore, T.K. Sinha, R. Taneja, D.N. Badodkar, M. Singh, S. Banerjee, Presented at Joint EC-IAEA Specialist meeting on NDT Methods for Monitoring Degradation, held at Petten, The Netherlands, 10–12 March 1999, p. 53.
[36] M. Singh et al., IAEA Tech. Committee Meeting, February 1994, Mumbai, India.
[37] R.I.K. Moorthy, J.K. Sinha, A.R. Rao, S.K. Sinha, A. Kakodkar, Nucl. Eng. Des. 155 (1995) 591.
[38] IAEA Tech. Committee Meeting on advances in safety related diagnostics and early failure detection, Vienna, 20–24 November 1995.
[39] D. Srivastava, G.K. Dey, S. Banerjee, Metall. Trans. A 26A (1995) 2707.
[40] V. Perovic, G.C. Weatherly, R.G. Fleck, Can. Metall. Q. 24 (3) (1985) 253.
[41] R. Dutton, The Met. Soc. CIM, Annual Volume (1978) 16.
[42] D.G. Westlake, J. Nucl. Mater. 26 (1968) 208.
[43] J.D. Eshelby, Proc. R. Soc. London (A) 241 (1957) 376.
[44] J.B. Bai, N. Ji, D. Gibon, C. Prioul, D. Francois, Metall. Mater. Trans. A 25A (1994) 1199.
[45] G.F. Slattery, J. Inst. Met. 95 (1967) 43.
[46] Z.L. Pan, I.G. Ritchie, M.P. Puls, J. Nucl. Mater. 228 (1996) 227.